Measurement of the electron-phonon coupling factor dependence on film thickness and grain size in Au, Cr, and Al

John L. Hostetler, Andrew N. Smith, Daniel M. Czajkowsky, and Pamela M. Norris

Femtosecond thermoreflectance data for thin films and bulk quantities of Au, Cr, and Al are compared with the parabolic two-step thermal diffusion model for the purpose of determining the electron-phonon coupling factor. The thin films were evaporated and sputtered onto different substrates to produce films that vary structurally. The measurement of the electron-phonon coupling factor is shown to be sensitive to grain size and film thickness. The thin-film thermoreflectance data are compared with that of the corresponding bulk material and to a theoretical model relating the coupling rate to the grain-boundary scattering and size effects on the mean free path of the relevant energy carrier. © 1999 Optical Society of America

OCIS codes: 120.5700, 240.0310, 260.3910, 350.5340.

1. Introduction

Nonequilibrium distributions between electrons and phonons in metals and superconductors are no longer limited to optical excitations, but are becoming increasing relevant in microelectronic devices processing high-frequency signals in the terahertz and subterahertz regime. Fast microwave devices such as thermal bolometers,[1] heterojunction bipolar transistors and heterojunction field-effect transistors[2] that exhibit nonequilibrium phenomena possess highly mobile free electrons that can counteract signal degradation and enlarge the region of lattice heating, thereby reducing peak lattice temperatures. This phenomena is seen in laser irradiation of mirrors where ultrashort laser pulses (<2 ps) can have higher fluences than longer pulses without irreversibly damaging the structure of the surface. These nonequilibrium features promise a future for terahertz devices, and accurate knowledge of the heat transfer mechanisms involved is imperative for the core design of such technology.

Generation of hot electrons in microwave devices can occur thermionically by the utilization of single or double potential barriers or through tunneling effects as in the tunneling electron hot electron amplifier.[2] Injection of hot electrons into the controlling region (the base) of microwave devices results in ballistic and quasi-ballistic electron transport through the base and collector. Quasi-ballistic electrons are hot electrons that suffer scattering during flight through the base whose length is typically less than the mean free path of the electron. Such devices have charging times as short as 500 fs, which can generate nonequilibrium distributions between the free electrons and the lattice. Characterization of the efficiency and performance of these devices is based on determining the amount of quasi-ballistic electrons in the distribution that suffer inelastic collisions that degrade mobility and thermalize the free carriers with the lattice. Knowledge of the rate of electron-phonon thermalization is a key component to characterizing the nature of quasi-ballistic electron distributions in microwave devices and is also used for determining peak lattice temperatures in mirrors used for ultrashort laser-pulse irradiation.

Nonequilibrium heating of metals at room temperature can be described by the parabolic two-step (PTS) thermal diffusion model. For ultrashort pulse laser heating, the PTS model accounts for photon

J. L. Hostetler, A. N. Smith, and P. M. Norris are with the Department of Mechanical and Aerospace Engineering, University of Virginia, Charlottesville, Virginia 22903. D. M. Czajkowsky is with the Department of Biophysics, University of Virginia, Charlottesville, Virginia 22903.

Received 26 October 1998; revised manuscript received 11 February 1999.

0003-6935/99/163614-07$15.00/0

© 1999 Optical Society of America

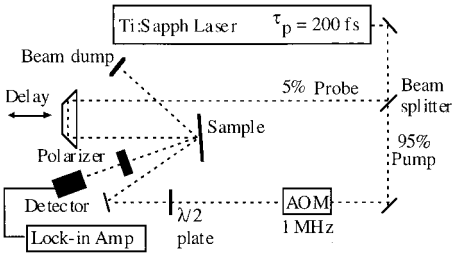

Fig. 1. Experimental setup. AOM, acousto-optic modulator.

absorption by free electrons and subsequent electron-lattice diffusion. The two coupled equations are given by[3]

$$C_e(T_e)\frac{\partial T_e}{\partial t} = \nabla[K(T_e)\nabla T_e] - G(T_e - T_l) + S, \quad (1)$$

$$C_l\frac{\partial T_l}{\partial t} = G(T_e - T_l), \quad (2)$$

where T_e and T_l are the electron and lattice temperatures, respectively; $C_e(T_e)$ and C_l are the volumetric heat capacity for the electron and lattice, respectively; $K(T_e)$ is the electron thermal conductivity; G is the electron-phonon coupling parameter that governs the rate of energy transfer to the lattice from the hot electrons; and S is the laser source term representing a Gaussian temporal pulse shape with constant optical properties.[4]

Measurement of the electron-phonon coupling parameter is typically accomplished through use of thermoreflectance methods, where the sample's reflectivity is monitored after the incidence of an ultrashort laser pulse.[5,6] The linear relationship between reflectivity and temperature results in a reflectance trace that can be compared with thermal relaxation models. This method is employed in this investigation to further study the dependence of the electron-phonon coupling factor on crystallinity and grain size and thickness for Au, Cr, and Al. The thermoreflectance responses of corresponding bulk materials were examined to compare with the thin-film results. Furthermore, a theoretical formulation of the coupling factor's dependence on scattering mechanisms developed by Qiu and Tien[7] is compared with experimental results and discussed.

2. Experimental Technique

A pump and probe experimental setup,[5,6,8,9] shown in Fig. 1, was employed to monitor the thermoreflectance response of each sample after the absorption of an ultrashort laser pulse (200 fs FWHM) of photon energy at 1.55 eV (λ = 790 nm). The pulses from a 76-MHz Ti:sapphire laser are separated into two beams with an intensity ratio of 95:5 by a nonpolarizing beam splitter. The intense pump beam (~6 nJ/pulse) is used to heat the film while the low-power probe beam is used to monitor the reflectivity. The pump beam passes through an acousto-optic modulator that effectively chops the beam on and off at a frequency of 1 MHz. The pump beam is focused to a diameter of ~40 μm at an incident angle of 30° off normal with an estimated fluence of <10 J/m^2. This creates a transient reflectance occurring at 1 MHz that is detected using a lock-in amplifier. The probe beam passes through a dovetail prism mounted on a movable stage that is used to increase the optical path length of the probe beam and hence the time delay between the pump and the probe pulses. The probe, which was centered in the heated area, is focused to ~5 μm at near-normal incidence to minimize the illuminated area. A half-wave retardation plate is used to rotate the pump beam's polarization to be orthogonal with the probe polarization. A polarizer with an extinction ratio of $\sim 10^{-6}$ is placed in front of the detector to filter out the scattered pump beam. A lock-in amplifier monitors the detector's response as the probe pulse is delayed in time, resulting in the temporal relaxation profile of the sample.

3. Experimental Considerations

Equations (1) and (2) were solved numerically using the Crank–Nicolson scheme with a uniform grid spacing of 0.5 nm and insulated boundary conditions. The temperature dependence of the electron heat capacity $C_e(T_e)$ and the thermal conductivity $K(T_e)$ are given by

$$C_e(T_e) = \gamma T_e, \quad (3a)$$

$$K(T_e) = K_{\text{eq}}\frac{T_e}{T_l}, \quad (3b)$$

where γ is the electron-specific heat constant[10] and K_{eq} is the thermal conductivity at equilibrium. The assumption of an insulated boundary at the film and substrate interface is validated by considering only the data within the first 2 ps, where the substrate effects have not yet affected the surface reflectivity. By monitoring only the center of the heated region with the probe, the radial diffusion in the film is neglected in the model. The one-dimensional assumption is valid in this investigation because the ratio of the width of the heated region to the penetration depth is $\sim 10^3$. To extrapolate the electron-phonon coupling parameter G from the data, the model is first multiplied by a constant that matches the magnitude of the thermoreflectance data to the PTS model and then the value of G is incremented using a curve-fitting routine written in LabView until a least-squares minimum is obtained. Furthermore, the PTS model is averaged over a Gaussian of 200 fs (FWHM) to account for the shape of the probing pulse's effect on the phenomena measured.

It is well known that the thermal conductivity $K(T_e)$ of thin metallic films suffers degradation because of size and structural effects. To overcome the need for accurate values of the reduced thermal conductivity, the diffusion term in Eq. (1) can be made negligible by fabricating the films with thicknesses approximately two times the optical penetration

depth (10–40 nm). This ensures that the film is volumetrically heated from the front surface to the film and substrate interface, and thermal diffusion within the film can be ignored. Although for nearly optically thin samples the diffusion term can be neglected, this is not the case for the bulk materials. This is accounted for in this study by assuming that the bulk samples of Au, Cr, and Al possess thermal diffusivities of published pure samples.

The assumption that pure ballistic transport of free electrons is negligible is based on the fact that the free electrons almost instantaneously reach the back side of the film, and the dominant process of relaxation is electron-phonon interaction. In bulk materials at low temperatures this assumption is subject to question; however, because of the high ambient temperature of the experiment (300 K), the effect is negligible.

The dependence of the optical properties on bound (lattice) and free electrons plays a significant role in the absorption and relaxation processes involved in short-pulse laser heating. The resulting thermal relaxation trace can be a convolution of both T_e and T_l, which is described by Brorson *et al.*[5] to be a linear relationship:

$$\Delta R = a\Delta T_e + b\Delta T_l, \tag{4}$$

where the parameters a and b describe how much the free and bound electrons affect reflectivity. It is well known that the reflectivity of metals is a function of photon energy, and contributions from free electrons through interband transitions and bound electrons through interband transitions create structure in the reflectance spectra.[11,12] This indicates that a and b are functions of photon energy and the complex dielectric function. If the pump beam is of a photon energy that excites both bound and free electrons, then absorption will occur in both systems. The small free electron to lattice heat capacity ratio ($\sim$0.01) will ensure nonequilibrium heating; however, the amount of nonequilibrium, i.e., $T_e - T_l$, will be affected. Determining the parameters a and b in Eq. (4) is the focus of a planned study by the authors in which wavelengths ranging from the UV to the near-IR will be used to compare theoretical expressions with experimental data. For purposes of measuring the parameter G, this obstacle can be overcome in two ways. The ratio a/b can be estimated by comparing the peak with the thermalization point after the fast free-electron transient has decayed away, or by considering only the data during the fast transient for curve-fitting purposes and comparing with T_e only. The second approach is valid because, immediately following the laser absorption, the fast transient is largely due to free-electron excitation and relaxation. The lattice temperature is small during this period and does not play a role until a few picoseconds after the absorption. The second approach is used in this investigation, and the results agree well with previous studies[5,6] where a/b was estimated. However, Al shows no fast transient free-electron spike in the early picoseconds of excitation, and the result is that aluminum's response to short-pulse heating is similar to the T_l profile. This aspect is discussed further in Section 5 where the aluminum data are presented.

After absorption of the laser pulse, a thermal expansion results that generates acoustic waves of ultrasonic frequency; therefore the resulting reflectance that is due to the thermal relaxation is also superimposed with the strain effects on reflectivity.[9] These strain effects can be significant depending on the material's thermal expansion, the photon energy, and the fluence of the heating beam. Furthermore, these effects can be seen in the first few picoseconds after absorption and can affect the measured G value. Studies were performed to characterize the strain effects for different fluence levels for Au and Cr for an incident photon of 1.55 eV. Gold shows little to no strain effects, even at higher fluences, but Cr shows that the strain effects are minimal at fluences around and below $\sim$9 J/m^2. The strain generation's dependence on material properties and photon wavelength indicates that this effect must be characterized for each sample before comparing data with thermal relaxation models. For example, ultrasonic effects were seen in the Al samples at fluences below 9 J/m^2, but were not present during the first few picoseconds, thus allowing the extrapolation of G.

4. Sample Preparation

The thin-film fabrication involved e-beam evaporation at 10^{-7} Torr and sputtering at relatively high pressures (10^{-3} Torr) onto several different substrates. All substrates were scrubbed with ethanol, trichloroacetic acid, and methanol prior to O_2 plasma cleaning and were placed immediately in the evaporation or sputtering chamber. The thin-film thicknesses were determined using a profilometer postdeposition and compared with the *in situ* oscillating crystal method, whereas grain size was characterized using an atomic force microscope (AFM). The AFM maps, shown in Figs. 2(a) and 2(b) two of the Au films and Fig. 3 for the Al film, indicate that all the films were polycrystalline. The average grain diameter was found by dividing a specified area by the number of grains in that area and assuming the grain's cross section to be circular.

Two sets of Au films were deposited onto single-crystalline Si and amorphous silica glass using evaporation and sputtering techniques. The evaporated samples were deposited to a thickness of 30 ($\pm$5) nm simultaneously at a rate of 1 Å/s. Figure 2(a) shows the topography of the evaporated Au on Si, where growth of smaller grains with an average diameter of $\sim$40 nm near the substrate surface and a layer of larger columnar grains ($\sim$100 nm) sparsely grown on top form two distinct stratified layers. An examination of the surface in several spots showed that these surface characteristics were constant in the region of interest, i.e., in the region of the optical measurement. The Au on the glass sample showed the same stratified layers and grain sizes, but had a larger

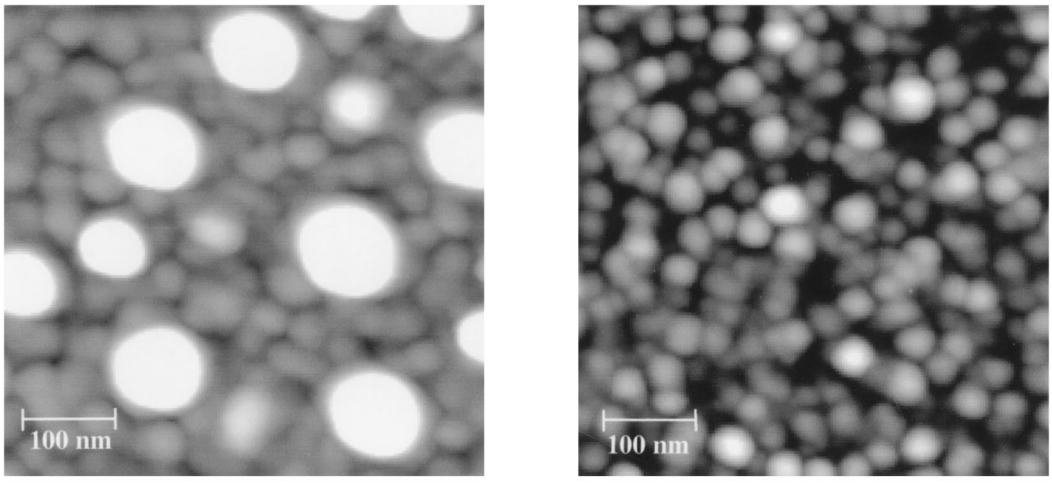

Fig. 2. AFM contrast maps of (a) evaporated Au on Si and (b) sputtered Au on glass.

number density for the large columnar grains grown near the free surface.

The sputtered samples were deposited simultaneously at a rate of 100 Å/min onto the same substrate materials as the evaporated samples to a thickness of 38 (±5) nm, as measured by a profilometer postdeposition. Figure 2(b) shows the AFM results for the sputtered Au on the glass sample. Both of the sputtered films showed no stratified effect, and the average grain diameter (~25–35 nm) was smaller than the evaporated samples.

The Cr and Al films were deposited by evaporation onto three different substrates simultaneously: single-crystalline Si, amorphous silica glass, and thermally grown SiO_2. The thermally grown SiO_2 was deposited on a single-crystalline Si wafer, and the thickness (634 nm) was measured using an interferometric technique[13] before the layer of Cr and Al was deposited. Profilometry measurements indicate that the Cr film thicknesses were ~51 (±5) nm whereas the crystal method indicated a thickness of 30 nm; however, the profilometer indicates an Al sample thickness of 13 (±5) nm, which agrees well with the crystal measurement of 12 nm. The profilometry measurements were used in calculations because of the frequent and large errors that vibrating crystals may produce. Figure 3 shows the evaporated Al on thermally grown SiO_2 sample where the average grain size is ~70 nm. The average grain diameter and film thickness for each sample are reported in Table 1 in Section 5.

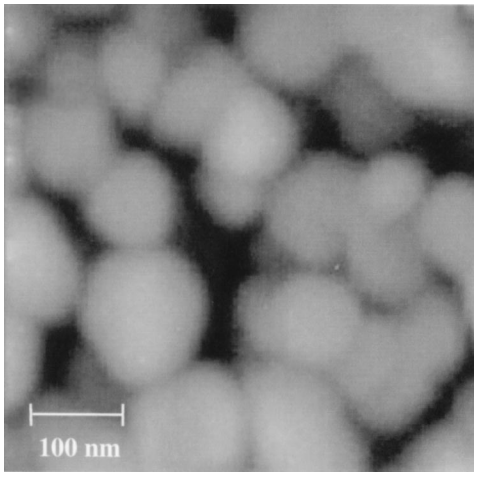

Fig. 3. AFM contrast map of evaporated Al on SiO_2.

Thick samples of highly pure Au (99.99%), Cr (99.97%), and Al (99.999%) were investigated to compare the thin-film thermoreflectance responses with those of the corresponding bulk materials. The blocks of Au, Cr, and Al were mechanically polished using a high-speed buffing wheel and jeweler's rouge and finishing polish until the surface had a near mirror finish. The samples were cleaned with acetone and methanol after polishing.

5. Results

The resulting values for G and the corresponding thin-film parameters are summarized in Table 1. Five scans were taken for each sample, and the value reported for G is the average and standard deviation of the extrapolated value. The fluence for each sample was approximately 7.5 (±1) J/m^2. The traces are normalized at the peak to compare the shape of the trace instead of the magnitude.

The thermoreflectance traces for the evaporated and bulk Au samples and the corresponding curve fits are shown in Fig. 4. During the first 200 fs, the absorption creates nonuniform electron temperature distributions, and the PTS is subject to question during this time.[14] For this reason, the data used in the curve-fitting routine was from the peak to ~1.5 ps and was fit with only the T_e profile. Although the thin-film traces are similar to the PTS model during this time, the traces for the bulk samples differ. The optically thin films are heated nearly uniformly dur-

Table 1. Measured Value of Thickness, Grain Size, and Electron-Phonon Coupling Factor

Material	Deposition Substrate	Thickness (nm) d ($\pm$5)	Grain size (nm) D ($\pm$10)	$G_{film} \times 10^{16}$ (W/m^3 K)
Au	Evaporated, glass	30	45	3.6 ($\pm$0.1)
	Evaporated, Si	30	37	4.4 ($\pm$0.2)
	Sputtered, glass	38	35	4.0 ($\pm$0.2)
	Sputtered, Si	38	27	5.0 ($\pm$0.2)
	Bulk	—	—	2.9 ($\pm$0.3)
Cr	Evaporated, glass	51	45	13.1 ($\pm$1.4)
	Evaporated, Si	51	35	13.6 ($\pm$1.8)
	Evaporated, SiO_2	51	55	10.0 ($\pm$0.4)
Al	Evaporated, glass	13	55	22.5 ($\pm$1.1)
	Evaporated, Si	13	35	20.1 ($\pm$0.8)
	Evaporated, SiO_2	13	70	22.7 ($\pm$0.4)
	Bulk	—	—	24.5 ($\pm$1.4)

ing the absorption, and this is believed to be the reason for the similar shapes; however, this is not the case in the bulk materials, and the results show deviations from the model during the absorption. The sputtered sample's response looks similar to the evaporated samples, so the data are not shown, but the value of G extrapolated is listed in Table 1. Inspection of the traces indicates that the heating for each sample is similar; however, the traces differ during the relaxation. The evaporated Au/Si has a higher average G value of 4.4 ($\pm$0.2) $\times$ 10^{16} W/m^3 K, evident by the steeper slope present just past the peak. This is believed to be due to the smaller average grain size ($D \sim 35$ nm) of the sample as compared with the evaporated Au/glass sample where the value of G extrapolated was 3.6 ($\pm$0.1) $\times$ 10^{16} W/m^3 K for a grain diameter of $D \sim 45$ nm. The same relationship can be seen with the sputtered samples where the Au/glass has a lower G value than the sputtered Au/Si, indicating a dependence of scattering mechanisms on substrate as well as deposition technique.

The reflectance trace for the bulk Au sample shows that the transient decay occurs on a shorter time

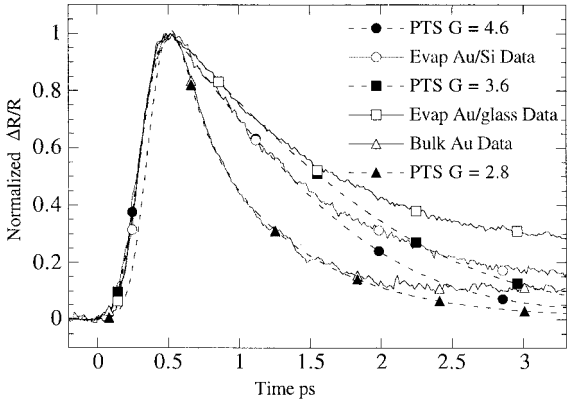

Fig. 4. Thermoreflectance traces of evaporated thin film and bulk Au where G is given in units of 10^{16} W/m^3 K.

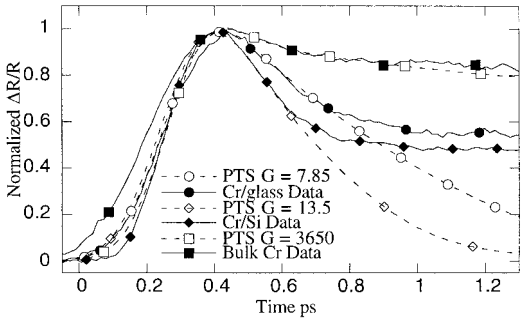

Fig. 5. Thermoreflectance traces and corresponding curve fits for evaporated thin film and bulk Cr where values of G are given in units of 10^{16} W/m^3 K.

scale than in the thin-film samples. This is expected as the diffusion term in Eq. (1) is no longer negligible and plays a significant role in the coupling of energy between the free electrons and the lattice by enlarging the affected region. The extrapolated value of G for the bulk sample is 2.9 ($\pm$0.3) $\times$ 10^{16} W/m^3 K.

The thin-film values for Au agree well with values reported by Elsayed-Ali *et al.*[6] and Orlande *et al.*[15] where it was found that polycrystalline Au films had a G of $\sim$4.0 $\times$ 10^{16} W/m^3 K. The bulk measurement of 2.9 $\times$ 10^{16} W/m^3 K agrees well with Brorson *et al.*,[5] but does not agree with the single-crystalline Au value reported by Elsayed-Ali *et al.* of 3.5 $\times$ 10^{16} W/m^3 K. This discrepancy could be due to the large number of dislocation densities reported by Elsayed-Ali *et al.* in the single-crystalline samples. The bulk sample in this investigation was a rolled sheet of Au, which typically possess large grains of the order of $\sim$1 μm in diameter, resulting in virtually no grain-boundary scattering.

Figure 5 shows the traces of the Cr samples on three different substrates. The thickness of the Cr films was found to be $\sim$50 nm. Because the optical penetration depth is $\sim$15 nm, there may be some diffusion occurring within the thin film. This was accounted for by including the diffusion term in Eq. (1) with a reduced value for conductivity that was calculated from a measurement of the electrical resistivity for evaporated Cr films on quartz substrates. Fouad *et al.*[16] reported a ratio of the thin-film resistivity to the bulk resistivity ρ_f/ρ_b of 1.15 for a 50-nm film. Assuming that the Wiedemann–Franz law holds in the thin-film regime,[17] the thermal conductivity ratio K_f/K_b yielded a conductivity of 83 W/m K. Extrapolating the G value for the reduced conductivity yielded a value that was reduced by 4% of the value using the bulk conductivity of 93.7 W/m K. The reduced value of conductivity was used in all the Cr thin-film analyses.

The fast transient data considered in the curve fit for the Cr samples was from the peak to $\sim$0.7 ps and compared with T_e only. The value of the coupling parameter measured here for all the thin-film Cr samples is lower than the value reported by Brorson *et al.*[5] of 42 $\times$ 10^{16} W/m^3 K. As can be seen in Fig.

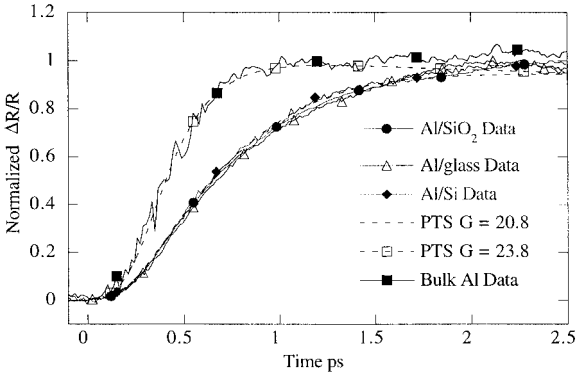

Fig. 6. Thermoreflectance traces and corresponding curve fits for evaporated thin film and bulk Al where values of G are given in units of 10^{16} W/m^3 K.

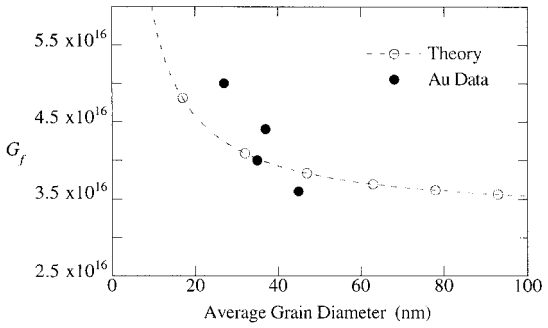

Fig. 7. Electron-phonon coupling factor for Au versus average grain diameter.

6, the extrapolated G is 3.65×10^{19} W/m^3 K for the bulk sample, which indicates that the excitation and relaxation are similar to the parabolic one-step model, where it is assumed that the laser energy is instantaneously absorbed by the lattice. This could be an artifact of the laser-pulse width, which may be considerably longer than the thermalization time for this sample. This enhancement of electron-phonon interaction could be due to the mechanical polishing of the bulk sample that may have introduced a thin layer of defects that significantly affected the initial absorption and dissipation of the radiation energy. For this reason the G value extrapolated for the bulk sample is subject to question and is not reported in Table 1.

The thermoreflectance traces for the four Al samples are shown in Fig. 6, and, as mentioned above, there is no fast transient free-electron spike. However, the resulting traces differ significantly from the parabolic one-step, where radiation energy is instantaneously absorbed by the lattice. This indicates that nonequilibrium heating is present.

There is a temporal lag of energy transfer from the laser pulse to the lattice, and the resulting traces are more similar to T_l than to T_e. The Fermi energy of Al (11.7 eV) is considerably higher than Au and Cr, and this results in a small amount of Fermi smearing induced by a photon of energy 1.55 eV, meaning that the reflectance is weakly dependent on T_e. There is also an interband transition peak[18] centered at the photon energy resulting in the absorption of radiation by the lattice as well as the creation of free electrons or excitons during the heating time, which are believed to create a loss during the excitation. In the Au and Cr analysis, G was measured by considering the energy loss from the free-electron system, whereas in the Al case, the value of G is measured by considering the gain of energy into the lattice. For these reasons the data were fit with the T_l profile and the value of G obtained as before. The data considered in this case are from 0 to ~2 ps so that substrate effects could be neglected and the ultrasonic effects are not yet significant. The three thin-film traces, as well as the bulk sample shown, yielded similar values for G, $\sim 21 \times 10^{16}$ W/m^3 K, indicating that the differences in traces are largely due to thin-film thickness rather than grain-boundary scattering. This is logical given the small film thickness (13 nm) and large grain diameter (~70 nm), indicating that the film is most likely one grain thick.

6. Discussion

The electron-phonon coupling factor for metal films G_f has been related to the mean free path of the free electron Λ_f through the consideration of the phonon emission and absorption probabilities and is given by the following expression[7]:

$$G_f = \frac{9}{16} \frac{nk^2 T_D^{\,2} v_F}{\Lambda_f T_l E_F}, \tag{5}$$

where n is the number density of electrons, k is Boltzmann's constant, T_D is the Debye temperature, v_F is the Fermi velocity, and E_F is the Fermi energy. To evaluate the effects of free-electron scattering off of film and grain boundaries, the mean free path of the film is related to the thin-film thickness d and the average grain diameter D through the following approximated expression[7]:

$$\Lambda_f = \frac{\Lambda_{e,b}}{1 + \frac{3\Lambda_{e,b}}{8d}(1 - P) + \frac{7}{5}\left(\frac{R_g}{1 - R_g}\right)\frac{\Lambda_{e,b}}{D}}, \tag{6}$$

where $\Lambda_{e,b}$ is the electron mean free path during electrical conduction in bulk materials, P is the specular reflection parameter of electrons at film surfaces, and R_g is the electron reflection coefficient at grain boundaries. The value of P is taken to be zero because of the very small wavelength of the free electron (~10 Å) that results in diffusive scattering only at thin-film boundaries. The value of R_g for Au is taken from empirical studies and is 0.17.[19] Using constants from Kittel,[10] Eq. (5) is plotted for Au in Fig. 7, where $d = 33$ nm and $\Lambda_{e,b} = 40$ nm. The data predict the magnitude and trend well, and it can be seen that for decreasing average grain diameter the electron-phonon coupling factor increases. The measured bulk value of $G = 2.9 \times 10^{16}$ W/m^3 K, not plotted,

indicates that the slope of G_f versus D flattens out as the grain diameter increases as predicted by Eqs. (5) and (6).

Because of the wide variability of published values of crucial parameters needed for Eqs. (5) and (6), the previous analysis is not possible for Cr at this time. However, the thermalization time t_c or the characteristic time of energy exchange between the free electrons and lattice can be estimated through the following simple formula[20]:

$$t_c = \frac{C_e}{G}, \tag{7}$$

where $C_e = 1.4 \times 10^4$ J/m^3 K.[10] The average value for the Cr measurements of $G = 12.2 \times 10^{16}$ W/m^3 K yields a thermalization time of 0.11 ps, which agrees well with the value reported by Qiu and Tien of 0.10 ps.[20]

The predicted G value of Al from Eqs. (5) and (6) yields a value of 69.9×10^{16} W/m^3 K for a grain size $D \sim 60$ nm and a film thickness of $d = 13$ nm. The empirical value of $R_g = 0.23$ (Ref. 19) and constants from Kittel[10] were used in the calculation. The resulting thermalization time for the Al samples is $\sim$0.19 ps, where $C_e = 4.1 \times 10^5$ J/m^3 K.[10]

The higher values of G for Cr and Al as compared with Au confirm the traditional belief that the chromium congener family and the trivalent main group metals have stronger electron-lattice interaction than the noble metals such as Au.

7. Conclusions

A thermoreflectance method was employed to investigate the dependency of the coupling of thermal energy from the free-electron system to the lattice in Au, Cr, and Al thin films on structural properties such as thickness and grain diameter. The presence of strain and its effect on the measurement were addressed. Nonequilibrium effects were seen in Al in which the resulting traces differ from the parabolic one-step model and behave similar to the lattice profile of the PTS diffusion model. The measured values of the electron-phonon coupling factor were compared with theory which accounts for size effects and grain-boundary scattering during thermal conduction, where the strength of coupling is seen to increase for decreasing average grain diameter.

References

1. P. Das, *Lasers and Optical Engineering*, 1st ed. (Springer-Verlag, New York, 1991).
2. K. S. Yngvesson, *Microwave Semiconductor Devices*, 1st ed. (Kluwer Academic, Norwell, Mass., 1991).
3. S. I. Anisimov, B. L. Kapeliovich, and T. L. Perelman, "Electron emission from metal surfaces exposed to ultrashort laser pulses," Sov. Phys. JETP **39,** 375–377 (1974).
4. T. Q. Qiu and C. L. Tien, "Femtosecond laser heating of multilayer metals. I. Analysis," Int. J. Heat Mass Transfer **37,** 2789–2797 (1994).
5. S. D. Brorson, A. Kazeroonian, J. S. Moodera, D. W. Face, T. K. Cheng, E. P. Ippen, M. S. Dresselhaus, and G. Dresselhaus, "Femtosecond room-temperature measurement of the electron-phonon coupling constant λ in metallic superconductors," Phys. Rev. Lett. **64,** 2172–2175 (1990).
6. H. E. Elsayed-Ali, T. Juhasz, G. O. Smith, and W. E. Bron, "Femtosecond thermoreflectivity of polycrystalline and single-crystalline gold films," Phys. Rev. B **43,** 4488–4491 (1991).
7. T. Q. Qiu and C. L. Tien, "Size effects on nonequilibrium laser heating of metal films," J. Heat Transfer **115,** 842–847 (1993).
8. C. A. Paddock and G. L. Eesley, "Transient thermoreflectance from thin metal films," J. Appl. Phys. **60,** 285–290 (1986).
9. J. L. Hostetler, A. N. Smith, and P. M. Norris, "Thin-film thermal conductivity and thickness measurements using picosecond ultrasonics," Micro. Thermophys. Eng. **1,** 237–244 (1997).
10. C. Kittel, *Introduction to Solid State Physics*, 7th ed. (Wiley, New York, 1996).
11. B. R. Cooper and H. Ehrenreich, "Optical properties of noble metals II," Phys. Rev. **138,** A494–A507 (1965).
12. H. Ehrenreich and H. R. Philip, "Optical properties of Ag and Cu," Phys. Rev. **28,** 1622–1629 (1962).
13. J. L. Hostetler, D. Stewart, C. E. Daitch, C. S. Ashley, and P. M. Norris, "Optical polarized reflectance characterization of thin aerogel and xerogel films," J. Non-Cryst. Solids **225,** 19–23 (1998).
14. D. Y. Tzou, *Macro- to Microscale Heat Transfer* (Taylor & Francis, Bristol, Pa., 1997).
15. H. R. B. Orlande, M. N. Ozisik, and D. Y. Tzou, "Inverse analysis for estimating the electron-phonon coupling factor in thin metal films," J. Appl. Phys. **78,** 1843–1849 (1995).
16. S. S. Fouad, A. H. Ammar, and M. H. El-Fazary, "A new approach to the correlation of the electrical properties with interband and intraband transitions of thin Cr films," Phys. Status Solidi, **187,** 99–108 (1995).
17. S. Kumar and G. C. Vradis, "Thermal conductivity of thin metallic films," J. Heat Transfer **116,** 28–34 (1994).
18. H. Ehrenreich, "The optical properties of metals," IEEE Spectrum **2,** 162–170 (1965).
19. J. W. C. De Vries, "Temperature and thickness dependence of the resistivity of thin polycrystalline aluminum, cobalt, nickel, palladium, silver and gold films," Thin Solid Films **167,** 25–32 (1988).
20. T. Q. Qiu and C. L. Tien, "Heat transfer mechanisms during short-pulse laser heating of metals," J. Heat Transfer **115,** 835–841 (1993).